ADVANCED ELECTRONIC MATERIALS
www.advelectronicmat.de

Enhanced N-Type Doping of a Naphthalene Diimide Based Copolymer by Modification of the Donor Unit

*Marco Cassinelli, Simone Cimò, Till Biskup, Xuechen Jiao, Alessandro Luzio, Christopher R. McNeill, Yong-Young Noh, Yun-Hi Kim, Chiara Bertarelli, and Mario Caironi**

Doped conjugated organic semiconductors are suitable materials to be used as building blocks of flexible and cost-effective thermoelectric generators. While several efficient solution-processable p-type organic thermoelectric materials are reported, n-doped materials are fewer because of lack of good electron-transporting materials and stable n-dopants. Here, n-doping process is investigated on a relevant n-type class, namely naphthalene-diimide-based copolymers. Among these, copolymer incorporating bithiophene (T2) donor units, largely studied poly{*N*,*N*″-bis(2-octyl-dodecyl)-1,4,5,8-naphthalenedicarboximide-2,6-diyl]-alt-5,5′-(2,2′-bithiophene)} (PNDI-T2), is one of first polymers reported to achieve good solution-based n-doping. By substituting T2 with thienylenevinylene-thienylene (TVT), resulting PNDI-TVT copolymer exhibits improvements on both structural and transport properties, offering a suitable basis to improve thermoelectric properties upon doping. When doped with 1*H*-benzimidazoles, PNDI-TVT achieves maximum in-plane electrical conductivity at room temperature of 2.4×10^{-2} S cm^{-1}, being the highest value for PNDI-T2 solution-doped derivatives excluding those with oligoethylene-glycol chains. Electron paramagnetic resonance and variable temperature electrical conductivity measurements relate this enhancement to more efficient charge-transfer between n-dopant molecules and host polymeric matrix, and easier charge carrier transport within the system. This electrical conductivity large enhancement also improves in-plane power factor of almost three times with respect to similar doped PNDI-T2 films.

1. Introduction

Thermoelectric (TE) devices are able to convert thermal energy into electrical power and vice versa, by exploiting the Seebeck and the Peltier effect, respectively.[1–7] Thus, depending on the device configuration, this technology can be used as TE generators (TEGs) or solid-state coolers (TECs), presenting several important advantages, such as pollution-free energy conversion, low-maintenance needs (due to the absence of moving fluids or mechanical parts in the system), long operational lifetime, no working noise, and easy scalability in size and power.[8–14] Despite these positive features, the widespread usage of the TE technology is limited since the building blocks of current commercial devices are based on inorganic materials,[15–19] which are more efficient, but also heavier, rigid, more expensive, and mostly based on rare and/or toxic elements.[20] In this framework, solution-processable doped conjugated polymers gained the interest of the TE research community,[20–32] since they are based on abundant nontoxic elements, possess easy tunable chemical structure,

M. Cassinelli, S. Cimò, A. Luzio, C. Bertarelli, M. Caironi
Center for Nano Science and Technology@PoliMi
Istituto Italiano di Tecnologia
Via Pascoli 70/3, Milano 20133, Italy
E-mail: mario.caironi@iit.it

The ORCID identification number(s) for the author(s) of this article can be found under https://doi.org/10.1002/aelm.202100407.

[+]Present address: Institut für Physikalische Chemie, Universität des Saarlandes, Campus B2 2, 66123 Saarbrücken, Germany

[++]Present address: National Synchrotron Radiation Laboratory, University of Science and Technology of China, No. 42 Cooperative South Road, Hefei, Anhui 230029, China

S. Cimò, C. Bertarelli
Dipartimento di Chimica
Materiali e Ing. Chimica "G. Natta"
Politecnico di Milano
Piazza L. Da Vinci 32, Milano 20133, Italy

T. Biskup[+]
Institut für Physikalische Chemie
Albert-Ludwigs-Universität Freiburg
Albertstraße 21, 79104 Freiburg, Germany

X. Jiao,[++] C. R. McNeill
Department of Materials Science and Engineering
Monash University
Clayton, Victoria 3800, Australia

Y.-Y. Noh
Department of Chemical Engineering
Pohang University of Science and Technology
77 Cheongam-Ro, Nam-Gu, Pohang 37673, Republic of Korea

DOI: 10.1002/aelm.202100407

low weight, mechanical robustness, and flexibility, thus being suitable as building blocks of flexible, light-weight, and cost-efficient organic thermoelectric generators (OTEG) fabricated on large scale by printing techniques.[20,33–36] The TE conversion efficiency of a given material is assessed through the dimensionless figure-of-merit: $zT = (S^2\sigma)T/(\kappa_e + \kappa_L)$, where S is the Seebeck coefficient, σ is the electrical conductivity, κ_e is the charge carrier thermal conductivity, κ_L is the lattice thermal conductivity of the material, and T is the absolute temperature. Compared to inorganic materials, organic semiconductors possess very low total thermal conductivity (κ), typically lower than 1 W m^{-1} K^{-1},[37,38] due to the intrinsic material structural disorder, suppressing the phonon component (κ_L).[39] Thus, the enhancement of organic TE performance is mainly related to the increase of the numerator of zT, namely the power factor ($PF = S^2\sigma$).[40]

Undoped organic materials show low electrical conductivity (in the range of 10^{-6} – 10^{-8} S cm^{-1}), corresponding to electrical resistances that are too high for the development of commercial devices.[28] However, by tuning the material charge carrier density through suitable doping processes, the material electrical conductivity can be enhanced.[37,38] At the same time, the material Seebeck coefficient decreases upon doping as the Fermi energy level approaches the transport energy level,[40–43] leading to a necessary compromise between high material electrical conductivity and power factor. Efficient and air stable p-type doped organic semiconductors based on doped poly(3,4-ethylenedioxythiophene) have been already widely reported, possessing a high in-plane PF of over 100 μW m^{-1} K^{-2}, leading to a promising zT of greater than 0.1.[44–47] Many efforts are still concentrated on the development of printable, efficient and air stable organic n-type doped materials whose performances remain below their p-type counterparts.[40,48–50] The difficulties lay on the very limited availability of efficient and environmentally stable electron-donating doping species,[51–55] as well as solution-doping strategies that are effective on electron-transporting organic semiconductors.[55–57]

Since the 1990s, studies on the n-doping process of semiconducting small molecule materials have been reported, investigating the correlation between the increase of the PF and both the doping conditions and the obtained material nanostructure.[42,58–65] Recently, an effective increase of the dopant miscibility was demonstrated through the replacement of the butric acid ester group with more polar oligo ethylene glycol side chains in solution processable n-doped [6,6]-phenyl-C_{61}-butyric acid methyl ester, leading to superior values of both in-plane σ (7 S cm^{-1}) and PF (≈47 μW m^{-1} K^{-2})[65] and also to an enhancement of the thermal stability of the doped materials.[42,64] Nonetheless, the ease of processability and printability from common organic solvents makes polymers more suitable for the fabrication of printed OTEGs. Among them, the most widely studied class of n-type organic material is the family of the naphthalene diimide (NDI)-based copolymers,[32,66–71] with the donor–acceptor (D-A) copolymer poly{*N*,*N*″-bis(2-octyl-dodecyl)-1,4,5,8-naphthalenedicarboximide-2,6-diyl]-alt-5,5′-(2,2′-bithiophene)}, here referred as PNDI-T2, being the most well-known example.[71,72] In several different studies, this copolymer was blended in solution with environmentally stable and solution-processable *1H*-benzimidazole *n*-dopants, such as (4-(1,3-dimethyl-2,3-dihydro-1*H*-benzoimidazol-2-yl)phenyl) (DMBI),[73–76] or *n*-doped by exposing to the vapor of strong reducing agents such as tetrakis(dimethylamino)ethylene (TDAE)[77] and highly branched polyethylenimine.[78] These strategies have led to values of in-plane σ in the range of 10^{-4} to 10^{-2} S cm^{-1}, but have achieved only moderate maximum in-plane PF values of ≈10^{-2} μW m^{-1} K^{-2}. Such low PF values, compared to p-type doped organic semiconductors, were initially ascribed to a limited dopant miscibility into the polymeric host caused by both the strong tendency of both to aggregate in solution and its semicrystalline nature.[33,74,79–81] Further studies related the limited doping efficacy to the presence of both a strong charge carrier intrachain localization on the distorted copolymer backbone[67,77] and to an intermolecular structural disorder,[82] typical of the D-A polymers.[82–86] As a result, torsion free polymers, characterized by a higher degree of delocalization, have been proposed as promising candidates for high performing n-type TE materials.[77] Moreover, since the lowest unoccupied molecular orbital (LUMO) of PNDI-T2 lies at an energy higher than the highest occupied molecular orbital (HOMO) of benzimidazole-derived dopants,[67,85,86] such as DMBI, the electron transfer process is hindered by an energy barrier which could be reduced by either slightly increasing the dopant HOMO or by reducing the polymer LUMO.

To overcome these issues, different structural modifications of the copolymer on the NDI-acceptor and/or T2-donor unit were reported. In particular, as in the case of small molecules, a large enhancement of σ was also reported in DMBI-doped-PNDI-T2 bearing polar oligoethylene-glycol side chains on both the NDI-acceptor[87] and the T2-donor unit.[88] The replacement of the polymer nonpolar alkyl side chains enhanced the compatibility of the organic semiconductors with the dopant molecules,[89] leading to a larger incorporation of the DMBI dopants and to an increased values of the in-plane σ of 0.17 S cm^{-1}, and in-plane PF of ≈0.4 μW m^{-1} K^{-2}.[87] A large enhancement of the σ was also achieved by replacing the NDI-core unit with perylene-diimide (PDI) unit, resulting in both a longer polaron delocalization length and a more electron-egative value of the polymer LUMO. The PDI-T2 copolymer, as doped with DMBI, reaches an in-plane σ values as high as 0.45 S cm^{-1}.[67] The T2-donor unit has also been modified with the bithiazole (Tz2) moiety.[90] Since Tz2 units possess a larger electron affinity than T2 units, this modification reduces the D-A character of the structure, lowering the LUMO of the polymer, but leaving the charge mobility similar to PNDI-T2.[90] Furthermore, the lower steric hindrance of Tz2 reduces the torsion angle between NDI and Tz2 units, leading to a more planar and conjugated structure. In fact, when doped with TDAE vapors, the PNDI-Tz2 copolymer exhibits higher values of both in-plane σ and PF of around 0.1 S cm^{-1} and 1.5 μW m^{-1} K^{-2}, respectively.[90–92]

Y.-H. Kim
Department of Chemistry and ERI
Gyeongsang National University
501, Jinju Daero 660-701, Republic of Korea

Herein, the n-type doping process of poly{(E)-2,7-bis(2-decyltetradecyl)-4-methyl-9-(5-(2-(5-methylthiophen-2-yl)vinyl) thiophen-2-yl)benzo[lmn][3,8]phenanthroline-1,3,6,8(2H,7H)-tetraone} (PNDI-TVT)[93] is investigated as a viable solution processable and highly electrical conductive n-type doped organic TE material. With respect to the parent moiety PNDI-T2, the presence of the thienylene-vinylene-thienylene (TVT) donor units leads to an increase of the crystalline structure of the copolymer films, resulting in a higher electron mobility value and a reduced bandgap, due to a large increase of the HOMO,[93] but leaving the LUMO almost unchanged.[93–99] The improved charge transport properties can be beneficial to overall enhance the electrical conductivity of the PNDI-TVT copolymer in the doped state compared with PNDI-T2 doped-copolymer. Thus, a different approach is here proposed in comparison with previous reports on solution-doped NDI-based copolymers where, in some cases, the structure of the backbone of the copolymer was specifically modified to enhance the interaction with the dopant,[33,67,90] and, in others, alkyl chains were modified by inserting for example polar oligoethylene-glycol side chains.[87,88,92] While in the case of the polar side chains a much higher PF is found, due to an enhanced carrier density, in both cases the carrier mobility results not improved with respect to PNDI-T2. Additionally, the n-doping process, carried out with benzimidazole derived dopants with linear and branched alkyl chain substituents,[76] results to be more efficient in PNDI-TVT n-doped films than in PNDI-T2 counterparts[76] as revealed by both electron paramagnetic resonance (EPR) spectroscopy measurements and by a detection of a lower electrical conductivity activation energy. As a result, a maximum value of the in-plane σ of 2.4×10^{-2} S cm^{-1} at room temperature (RT) is achieved which is almost four times larger with respect to both similar n-doped PNDI-T2[76] and to DMBI-doped PNDI-Tz2.[90] Furthermore, a threefold improvement in the in-plane PF of 3.9×10^{-2} μW m^{-1} K^{-2} with respect to PNDI-T2 doped-films is also achieved.[76] This work evidences how a subtle effect of molecular structure can positively influence the thin film TE properties of doped polymers for a representative class of good electron transporting and printable materials, i.e., NDI-based copolymers. From understanding the relationship between molecular structure and doping, successful doping and processing strategies can be devised providing a pathway toward efficient and cost-effective OTEGs. In fact, although the here presented results are still limited, our work demonstrates clear advances in both the performance and the comprehension of more effective strategies to enhance thermoelectric properties of the NDI-based polymers.

2. Results and Discussion

Figure 1 shows the molecular structure of the PNDI-TVT copolymer and the four different 1*H*-benzimidazole-based molecules used as n-dopants in this work. DMBI is a well-known and well-studied molecule.[100,101] *N*,*N*-dibutyl-4-(1,3-dimethyl-2,3-dihydro-1*H*-benzo[*d*]imidiazol-2-yl)aniline (DBuBI) is a derivative of DMBI possessing long linear n-butyl substituent chains, while 4-(1,3-dimethyl-2,3-dihydro-1*H*-benzo[*d*] imidazole-2-yl)-*N*,*N*-diisopropylaniline (DiPrBI) and 4-(1,3-dimethyl-2,3-dihydro-1H-benzo[d]imidazole-2-yl)-*N*,*N*-diisobutylaniline (DiBuBI) possess branched alkyl substituents of different size.[76] In order to investigate the effects of the dopants on the electrical, optical, and morphological properties of the polymer, aliquots of each dopant, dissolved in anhydrous dichlorobenzene (DCB), were separately added to PNDI-TVT solutions, thus varying systematically the dopant molar ratio. The dopant molar ratio (mol%) is defined as the moles of dopant divided by the number of polymer repeating units. The films were then

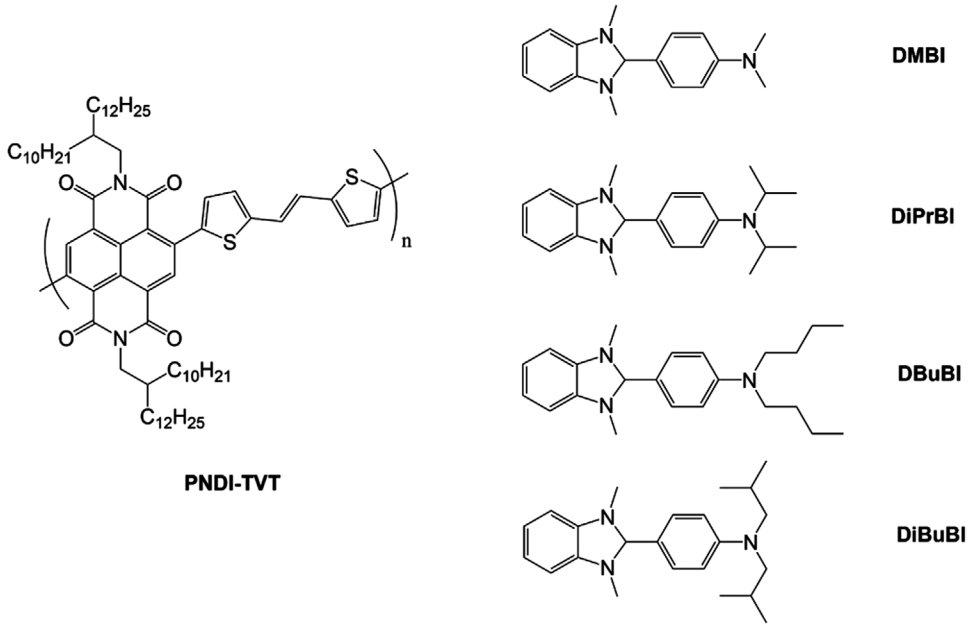

Figure 1. Molecular structure of PNDI-TVT and *N*-alkyl substituted 1*H*-benzimidazole dopants.

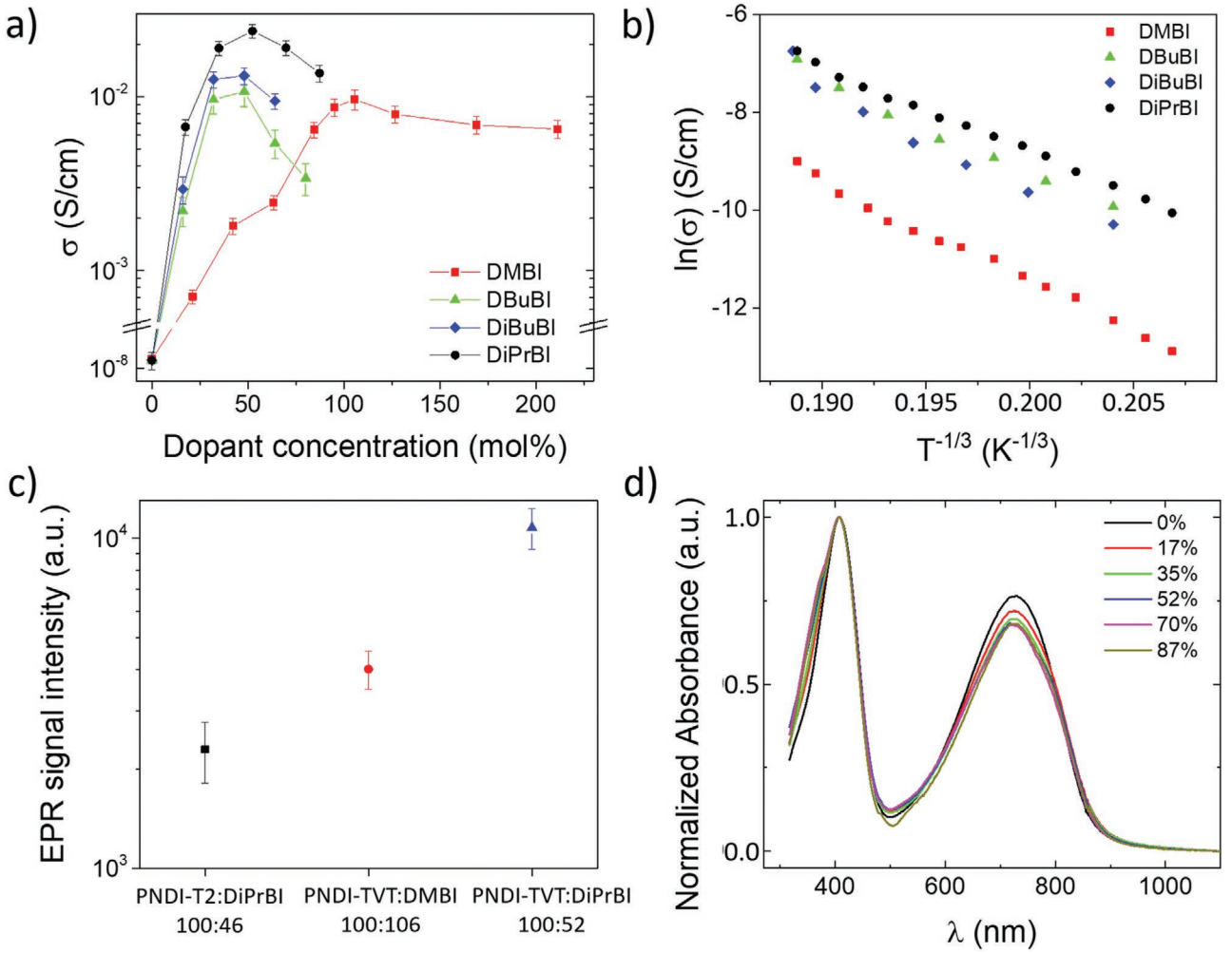

Figure 2. a) In-plane electrical conductivity (σ) versus dopant molar ratio (mol%) of PNDI-TVT doped with *N*-alkyl substituted 1*H*-benzimidazoles. b) Temperature dependence of the in-plane σ between 190 and 300 K for PNDI-TVT doped with the four different dopants with the dopant concentration showing the best value, namely 106% for DMBI, 48% for both DBuBI and DiBuBI, and 52% for DiPrBI. c) EPR signal intensity (double integral) averaged for three orientations of the substrate with respect to the external magnetic field (0°, 45°, and 90°) obtained for PNDI-T2 doped with 46 mol% DiPrBI (black square), PNDI-TVT doped with 106 mol% DMBI (red circle) and with 52 mol% DiPrBI (blue triangle). d) UV–vis–near-IR absorption spectra of PNDI-TVT thin films doped in solution with different concentration of DiPrBI.

prepared with a procedure identical to that reported by Saglio et al., used for the investigation of doped PNDI-T2 films with the same dopant molecules series,[76] allowing then a direct comparison of the values of both σ and S here measured. First, to confirm the good transport properties of the PNDI-TVT material batch used in this work, the copolymer charge carrier mobility was measured in a top-gate, bottom-contact field-effect transistor (FET) configuration, achieving a value of 1.5 $cm^2\ V^{-1}\ s^{-1}$, similar as the value reported in literature using an identical geometry[93] (see Figure S1, Supporting Information).

Figure 2a reports the values of the in-plane σ of the doped PNDI-TVT films with four different dopant molecules, for a concentration ranging from 0 to 200 mol%. The values were extracted through the method reported in the Supporting Information. The maximum detected σ values are $(9.7 \pm 0.9) \times 10^{-3}$ S cm^{-1} for 106% DMBI, corresponding to a 25% concentration expressed as weight ratio of the dopant-to-polymer w/w, $(1.1 \pm 0.2) \times 10^{-2}$ S cm^{-1} for 48% DBuBI, $(1.3 \pm 0.2) \times 10^{-2}$ S cm^{-1} for 48% DiBuBI, and $(2.4 \pm 0.3) \times 10^{-2}$ S cm^{-1} for 52% DiPrBI, all corresponding to 15% w/w concentration. These results confirm the higher doping efficiency of the molecules carrying longer alkyl linear chains, as in case of DBuBi, and bearing alkyl branched chains, as for DiBuBi and DiPrBi, with respect to DMBI molecules, as also reported by Saglio et al.[76] for the doped PNDI-T2 films. Moreover, the σ detected in DiPrBI-doped PNDI-TVT presents a value which is ten times greater than the reported for DMBI-doped PNDI-T2 ($\approx 1.8 \times 10^{-3}$ S cm^{-1}),[76] and almost four times greater than for both DiPrBi-doped PNDI-T2[76] and DMBI-doped PNDI-Tz2 ($\approx 7 \times 10^{-3}$ S cm^{-1}),[90] being the highest σ value achieved by solution-doping of PNDI-T2 derivatives without carrying polar oligoethylene-glycol side chains. Moreover, the σ values as a function of the dopant concentration follow a similar trend for all the four different dopants: σ initially increases, reaching a maximum in between 48% and 106% dopant concentration, and then decreases for higher mol%. This decrease

can be related to the dopant phase segregation in the system, hindering hinders the further enhancement of σ as increasing the dopant concentration in the system,[74] and an investigation of this possible effect is later reported.

First, to better understand this enhancement, the transport properties of the doped thin films were investigated by evaluating the activation energy (E_a) of the in-plane σ. This was obtained by measuring the temperature dependence of σ for the different doped films between 190 and 300 K, reported in the Arrhenius plot in Figure 2b. As notable, in all cases σ decreases as the temperature drops, with the best fit following a temperature dependence as $\ln \sigma(T) \propto T^{-1/3}$ (see Figure S2, Supporting Information), typical of a 2D variable range hopping transport regime.[62] Such simple fitting should be considered only indicative, and not evidence for a precise physical model, for which at least coulombic effects related to presence of dopant counterions should be considered.[42,102] Nevertheless, the Arrhenius plot strongly suggests that both the conduction regime and the energetic structure remain identical for all the doped systems, thus not affected by the different dopant molecules, despite the differences in σ. In fact, using the best fit, the E_a of the doped systems is estimated[103] $\approx 270 \times 10^{-3}$ eV in all cases. This evidence suggests that the differences in the σ values are related to an increase of the charge carrier density (n) as a function of the dopant. Similar measurements performed on PNDI-T2 doped with the same molecules reported higher value of E_a of $\approx 330 \times 10^{-3}$ eV,[76] thus suggesting a more efficient charge transport in PNDI-TVT systems.[93,104]

To corroborate the hypothesis of a different charge carrier density in differently doped PNDI-TVT films, samples doped with 52% DiPrBI and with 106% DMBI were then investigated by continuous-wave EPR spectroscopy. Furthermore, to compare the results with the parent material, PNDI-T2 films doped with 46% DiPrBI (25% w/w concentration), percentage at which the maximum of σ was detected,[76] were also analyzed. Generally, the double integral of the original, first-derivative cw-EPR signal is proportional to the number of paramagnetic centers in the sample. The results of the semiquantitative analysis averaging over three orientations of the substrate with respect to the external magnetic field (0°, 45°, and 90°) are reported in Figure 2c. As visible, the EPR signal intensity is larger in both the PNDI-TVT doped systems with respect to the PNDI-T2 films (see also Figure S3, Supporting Information), achieving the highest value for the sample doped with DiPrBI, consistent with the σ measurements. Comparing the results for the TVT-based copolymer, the larger signals detected for the DiPrBi doped system with respect to the DMBI film confirm the increased polymer-dopant interaction for the bearing alkyl branched chains dopants,[76] leading to a higher carrier density (n) in the former doped film (see also Figure S4, Supporting Information). Thus, the larger measured values of σ for PNDI-TVT doped samples with respect to PNDI-T2 adding similar percentage of DiPrBi molecules are related to both the system higher detected charge carrier density, revealing a more efficient charge transfer between the n-dopant small molecules and the host polymeric matrix, and the improved charge transport properties.[93]

To get more insights into these results, the polymer conformation/microstructure evolution of the doped PNDI-TVT as a function of the dopant concentration for the four different molecules was analyzed first by UV–vis measurements on the thin films prepared with same procedure as for the σ measurements, with the data of the DiPrBI doped system reported in Figure 2d. All the spectra show the two main peaks associated to a π–π^* transition, at 403 nm, and to an intramolecular charge transfer (ICT), at 716 nm, caused by the D-A structure of the copolymer.[93,105] Increasing the dopant concentration in the system causes mainly a reduction of the intensity of both the detected peaks, leading to an overall reduction of the intensity for both the π–π^* and ICT transition, and a decrease of the relative intensity of the ICT peak over the π–π^* peak, as already reported in 4-(1,3-dimethyl-2,3-dihydro-1H-benzoimidazol-2-yl)-N,N-diphenylaniline doped PNDI-T2 films.[86] Analogous results were obtained also using the other dopant molecules (see Figure S5, Supporting Information), suggesting the absence of any evolution of the molecular microstructure as a function of any used benzimidazole derivative dopants. Therefore, similar to DMBI-doped PNDI-T2 films,[78] the inclusion of dopant molecules does not appear to significantly alter the local molecular environment, and by extension is not expected to significantly modify the molecular packing.[93] To further investigate this result, synchrotron-based grazing incidence wide-angle X-ray scattering (GIWAXS) measurements were performed on PNDI-TVT thin films doped with an increasing amount of DiPrBI. The 2D GIWAXS data plots with the corresponding 1D profiles are reported in **Figure 3**. The pristine film is characterized by a series of lamellar stacking reflections (h00) up to the fifth order, scattering primarily in the out-of-plane direction, indicating a predominantly edge-on orientation of the crystallites. However, a distribution of crystallites orientations is evident by the "arcing" of the detected peaks as well as a backbone reflection (001) which is detected in the in-plane direction at a q-value of ≈ 4 nm^{-1}. All these features are consistent with previous GIWAXS results reported for undoped PNDI-TVT films.[96] For doping with DiPrBI molecules at 17%, the peak width of the lamellar stacking peak increases, indicating a decrease in crystals size and/or an increase in crystalline disorder. Table S1 in the Supporting Information summarizes the parameters obtained from fitting of the (100) lamellar stacking peak confirming that doping leads to a decrease in the coherence length from ≈400 to ≈300 Å along with a slight increase in d-spacing from 27.2 to ≈27.6 Å. In the doped film, a prominent in-plane lamellar stacking peak is also seen, indicating that in doped samples there is the copresence of both edge-on and face-on crystallites, though the predominant crystal orientation remains edge-on. The presence of this mixed morphology is reported to enhance the transport properties of the system compared to the 100% edge-on configuration.[93] As increasing the dopant concentration to 52%, new peaks appear in the in-plane line profile, indicating the probable phase-segregation of the dopant molecules. Despite this effect, the positions of the PNDI-TVT peaks remain constant for all the samples, confirming that the dopant does not induce any changes of the packing of PNDI-TVT chains, in agreement with the UV–vis measurements, although the presence of the dopant molecule does affect the crystallites size/order and orientation.

To collect data about the possible dopant phase-segregation in the PNDI-TVT system, the film microstructure was further analyzed by atomic force microscopy (AFM) through the

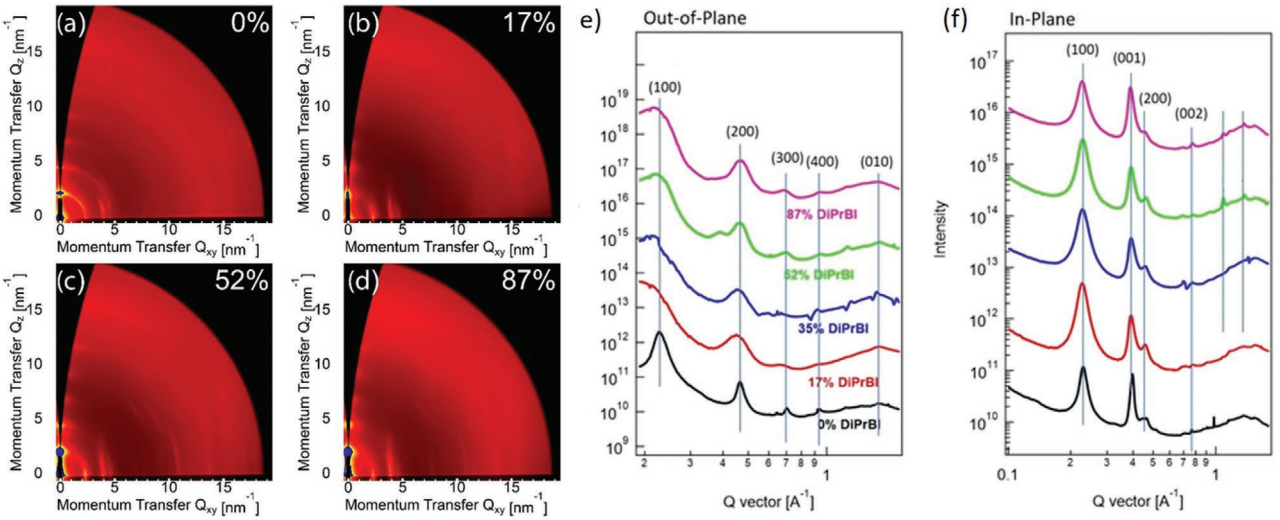

Figure 3. (Left) 2D GIWAXS data plots of PNDI-TVT films doped with DiPrBI at different dopant concentrations (mol%): a) 0%, b) 17%, c) 52%, and d) 87%. (Right) The corresponding 1D GIWAXS line profiles taken along e) the out-of-plane and f) the in-plane scattering directions.

imaging of sample surface topography. The images are reported in **Figure 4** along with the relative root mean square roughness (R_{RMS}). The pristine PNDI-TVT film in Figure 4a exhibits the typical fiber-like morphology, similar to pristine PNDI-T2,[76] with a value of R_{RMS} of about 0.9 nm. By adding DiPrBI and DiBuBI dopants to the system, the surface presents round features, as visible in Figure 4b,c, and an increased value of (R_{RMS}) of 1.83 and 1.27 nm, respectively, providing more evidences for the presence of dopant segregation, which could help to explain the observed decrease of σ at high dopant concentration measured in all the doped systems.

Finally, **Figure 5** reports the measurements of the in-plane S, σ, and PF of the DiPrBi-doped PNDI-TVT films as a function of the doping concentration from 17% to 70% at 413 K, considering possible applications at slightly higher temperature than RT. The σ measurements confirm the trend of the RT values, with the 52% sample being the most conductive film with a value of (0.12 ± 0.02) S cm^{-1}. The measured S values are always negative, as expected for systems dominated by electrons, thus confirming the n-doping effect of the 1*H*-benzimidazole molecules on the copolymer. In particular, the values drop from −129 to −12 μV K^{-1} as the dopant concentration increases, confirming the increase of the charge carrier density n in the system. However, the theoretical inverse proportionality between S and σ, i.e., $S \propto \sigma^{-1/s}$, where s is equal to 3 or 4 in most cases in polymer system,[40,41,88] due to shifting of the Fermi level toward the conduction band as a consequence of the doping,[106,107] is not observable for the sample doped at 70%. In this case, the presence of the dopant phase segregation leads to an overall decrease of the total σ, but this is not correlated with the expected increase of S.[108] This behavior suggests a dominant role of the reduced mobility in the drop of σ at such high doping concentration, not affecting S.[106,107] The calculated PF of the DiPrBi-doped PNDI-TVT at 413 K achieves a maximum value of 0.103 μW m^{-1} K^{-2} for the lowest investigated dopant concentration due to the highest detected value of the Seebeck coefficient.

Moreover, for the 52% DiPrBI-doped system, σ and S were also measured at 353 K, giving as results $(4.9 \pm 0.9) \times 10^{-2}$ S cm^{-1} and −(24 ± 8) μV K^{-1}, respectively, leading to a total PF of $(2.9 \pm 0.8) \times 10^{-3}$ μW m^{-1} K^{-2}. This value is almost three times higher than the best PF obtained in PNDI-T2 films with 76%

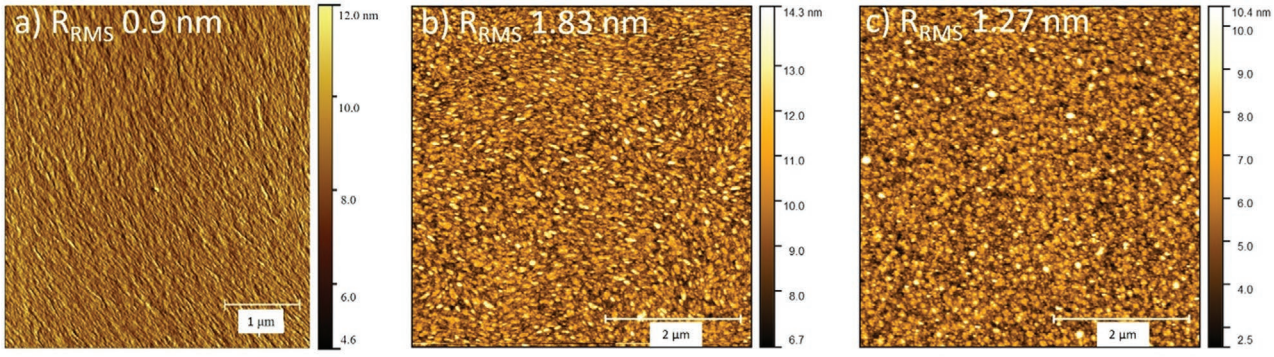

Figure 4. Atomic force microscopy (AFM) scans of the a) undoped PNDI-TVT, b) PNDI-TVT doped with 48 mol% DiBuBI, and c) with 52 mol% DiPRBI, with the relative measured values of the root mean square roughness (R_{RMS}).

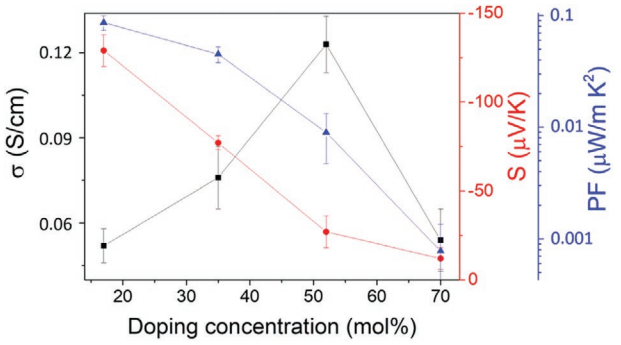

Figure 5. In-plane electrical conductivity (σ), Seebeck coefficient (S), and power factor (PF) versus dopant molar ratio (mol%) of PNDI-TVT doped films with different concentrations of DiPrBI (from 17 to 70 mol%) at 413 K.

DiPrBI, ($\approx$1.1 × 10^{-3} μW m^{-1} K^{-2}), measured at similar temperature,[76] confirming the enhancement of the TE properties in doped-PNDI-TVT. In particular, this increased value of PF is related to the larger σ values achieved in PNDI-TVT n-doped samples compared to the PNDI-T2 n-doped films,[76] since slightly higher values of S were measured in the *n*-doped PNDI-T2 system.[76] The larger σ values measured for PNDI-TVT doped samples with respect to PNDI-T2 ones, adding similar percentage of DiPrBi molecules, are then related to both the larger charge carrier density detected by EPR measurements, revealing a more effective n-doping process with 1*H*-benzimidazoles small molecules than in PNDI-T2 polymer, and the improved electron transport properties characterizing PNDI-TVT.[93] Such increase in σ, without largely sacrificing the system S, results in an overall enhancement of the PF. These results also underline the not trivial interdependence between the transport properties of the systems, namely the electron mobility and electrical conductivity, and the Seebeck coefficient.[107]

3. Conclusions

In summary, the TE properties of PNDI-TVT copolymer thin films n-type doped with 1*H*-benzimidazoles dopants carrying different *N*-alkyl substituents have been here investigated. Thanks to the presence of the TVT donor unit, modified with respect to the PNDI-T2 parent moiety, PNDI-TVT presents superior charge transport mobility in the pristine form, offering a suitable basis for improved TE properties upon doping. In fact, the copolymer achieves a maximum in-plane σ of 2.4 × 10^{-2} S cm^{-1} at RT, which is almost ten times greater than the reported for DMBI-doped PNDI-T2,[76] and almost four times greater than for both DiPrBi-doped PNDI-T2[76] and DMBI-doped PNDI-Tz2,[90] making it the highest σ value achieved by solution-doping in PNDI-T2 derivatives excluding those carrying polar oligoethylene-glycol side chains. From EPR and variable temperature electrical conductivity measurements this enhancement is related to a more efficient charge transfer between the n-dopant molecules and the host polymeric matrix as well as to the improved transport properties of the charge carriers in the PNDI-TVT system. However, as expected, the increase of the charge carrier concentration in the PNDI-TVT doped-films leads to a slightly lower Seebeck coefficient, in comparison to doped PNDI-T2 films at similar temperature.[76] Nevertheless, the large enhancement of the electrical conductivity also improves the in-plane power factor of PNDI-TVT doped-films by almost three times with respect to PNDI-T2 doped-films at similar temperature,[76] achieving a value of (2.9 ± 0.8) × 10^{-3} μW m^{-1} K^{-2}. These results confirm that superior electrical properties can be achieved in D-A copolymers by appropriate structural modification, promoting both the polymer transport properties and efficient n-doping process.

4. Experimental Section

Materials: PNDI-TVT were synthesized according to published procedures.[93] The PNDI-TVT batch used in this experiment possessed the same molecular weight (M_n = 70 kDa), dispersity (M_w/M_n = 1.98) and chemical composition as previously reported.[93] The molecular weights and the dispersity of the copolymers were determined by gel permeation chromatography (GPC) analysis with polystyrene standard calibration (Waters high-pressure GPC assembly Model M515 pump, u-Styragel columns of HR4, HR5, with 2414 refractive index detectors, solvent: $CHCl_3$). All the 1*H*-benzimidazoles with the *N*-alkyl substituents were synthesized according to published procedures.[76]

Solutions Preparation: PNDI-TVT were dissolved in 1,2-DCB at a concentration of 5 g L^{-1} at RT and used after 12 h of dissolution. 1*H*-benzimidazoles dopants were prepared at concentration of 5 g L^{-1} and used after 12 h of dissolution at RT. Aliquots of polymer and dopant solution were mixed and stirred for 10 min at RT just before the deposition.

Thin Films Preparation: Low-alkali 1737F Corning glasses were used as substrate and they were cleaned in ultrasonic bath of Milli-Q water, acetone, and isopropyl alcohol, 10 min for each step. Then, the substrates were exposed to O_2 plasma at 100 W for 10 min. By a shadow mask, electrodes of a 1.5 nm thick Cr adhesion layer and 25 nm thick Au film were obtained by thermal evaporation. Thin polymer films were then spin-cast from solutions onto the substrates, in a nitrogen filled glovebox at 1000 rpm for 60 s and annealed at 150 °C for 6 h in inert atmosphere, with an average thickness of (43 ± 7) nm, not apparently influenced by the different dopants and dopant concentrations, as visible in Figure S6 in the Supporting Information.

Electrical Characterization: The *I–V* curves were measured at RT in N_2 atmosphere in two-point contact method with a Wentworth Laboratories probe station with a semiconductor device analyzer (Agilent B1500A). The *I–V* curves detected at low temperatures were measured in N_2 atmosphere in two-point contact method with a Keysight Technologies semiconductor parameter analyzer. The in-plane electrical conductivity was then calculated through the linear fit of the *I–V* data, the thin films geometry, and thickness, obtained with an alpha-step IQ profilometer from KLATencor.

FET: Bottom gold contacts (30 nm) were fabricated on glass substrates using conventional photolithography, yielding transistor channels with a length L = 20 μm and a width W = 10 mm. The semiconducting polymer was dissolved in chlorobenzene at a concentration of 10 mg mL^{-1}, and spin coated at 2000 rpm for 60 s. After deposition the samples were annealed at 180 °C for 10 min starting from RT and gradually increasing the temperature by 10 K min^{-1} and then slowly cooled down to RT. Then poly(methylmethacrylate), dissolved in *n*-butyl acetate (concentration 80 mg mL^{-1}), was spin coated at 2000 rpm for 60 s, yielding to 600 nm thick dielectric layer, followed by an annealing at 80 °C for 2 h to remove the solvent residuals. Finally, a 50 nm thick aluminum layer was deposited on the channel area by thermal evaporation. Devices were then annealed at 130 °C in nitrogen atmosphere for 12 h. The samples were fabricated and measured in a nitrogen atmosphere.

UV–vis–Near IR Measurements: UV–vis–near IR measurements were carried out on a PerkinElmer λ1050 spectrophotometer, using a tungsten lamp as source.

EPR Measurements: Thin films were prepared in inert atmosphere by spin-coating 10 µL of solution (concentration of 5 g L^{-1}) onto synthetic quartz glass substrates (Ilmasil PS, QSIL GmbH) with dimensions of 3×25 mm^2, followed by annealing at 150 °C for 4 h. Then, the annealed films were placed into synthetic quartz glass tubes (Ilmasil PS, QSIL GmbH) with 3.8 mm outer and 3.0 mm inner diameters and the tubes sealed afterward. EPR spectra were recorded at RT on an Elexsys 580 (Bruker Biospin GmbH) spectrometer equipped with a 4119HS-W1 (Bruker) cavity: microwave frequency, 9.800 GHz; microwave power, 150 µW (30 dB attenuation, 150 mW source power); modulation frequency, 100 MHz; modulation amplitude, 0.1 mT. Semiquantitative analysis has been performed by doubly integrating the original first-derivative data and by averaging over the signal intensities obtained for three orientations of the substrate with respect to the external magnetic field (0°, 45°, and 90°).

Atomic Force Microscopy: The thin polymer investigated by AFM was prepared using the same procedure described in the Experimental Section. The surface morphology of the films was detected by an Agilent 5500 atomic force microscope, operating in acoustic mode.

GIWAXS: GIWAXS experiments were conducted at the SAXS/WAXS beamline at the Australian Synchrotron[96] using 12 keV photons, with the 2D diffraction patterns collected by a Dectris Pilatus 2M detector. Images taken at the critical angle were used for further data analysis, with the critical angle identified by scanning the X-ray angle of incidence from 0° to 0.15° with intervals of 0.01°. The X-ray exposure time was chosen as 1 s to maximize signal to noise ratio and in the same time minimize beam damage. Gapless mode of Pilatus 2M detector was utilized to eliminate the blank gap intrinsic to the detector. The Pilatus 2D detector was under vacuum in a flight tube. The sample stage was set within a separate vacuum chamber. Silver behenate was used as the diffraction standard to calibrate the physical dimension of detector-sample distance and beam center position. Data analysis is performed in Igor pro with a customized version of the Nika code.[109]

Seebeck Measurements: The in-plane Seebeck coefficient as well as the electrical resistance of the thin films was measured in a homemade setup reported by Beretta et al.[110] The measurements were performed at 10^{-4} mbar vacuum, to avoid convection phenomena and to preserve the polymer electrical properties. The in-plane electrical conductivity was then calculated through the thin films geometry and thickness, obtained with an alpha-step IQ profilometer from KLATencor.

Supporting Information

Supporting Information is available from the Wiley Online Library or from the author.

Acknowledgements

M.C. wants to thank E. Sarta (Istituto Italiano di Tecnologia, Italy) for the precious support and discussion during the measurements. This work was performed in part of the Australian Nuclear Science and Technology Organisation (ANSTO). T.B. acknowledges S. Weber (University Freiburg, Germany) for providing EPR equipment. The work was partly supported by the National Research Foundation of Korea (NRF) (2018R1A2A1A05078734). This study was also supported by Ministry of Science and Information, Communication and Technology through the National Research Foundation (NRF) grant, funded by the Korea government (2020R1A4A1019455).

Open access Funding provided by Istituto Italiano di Tecnologia within the CRUI-CARE Agreement.

Conflict of Interest

The authors declare no conflict of interest.

Data Availability Statement

Research data are not shared.

Keywords

conjugated polymers, NDI copolymers, n-type doping, organic thermoelectrics, polymer conductors

Received: April 20, 2021
Revised: June 29, 2021
Published online: August 8, 2021

[1] D. M. Rowe, *Thermoelectrics Handbook: Macro to Nano*, Taylor and Francis, New York **2006**.
[2] L. E. Bell, *Science* **2008**, *321*, 1457.
[3] J. R. Szczech, J. M. Higgins, S. Jin, *J. Mater. Chem.* **2011**, *21*, 4037.
[4] M. Cassinelli, S. Müller, K.-O. Voss, C. Trautmann, F. Völklein, J. Gooth, K. Nielsch, M. Toimil-Molares, *Nanoscale* **2017**, *9*, 3169.
[5] J. Yang, F. R. Stabler, *J. Electron. Mater.* **2009**, *38*, 1245.
[6] M. Cassinelli, A. Romanenko, H. Reith, F. Volklein, W. Sigle, C. Trautmann, M. E. Toimil-Molares, *Phys. Status Solidi A* **2016**, *213*, 603.
[7] M. Cassinelli, S. Müller, Z. Aabdin, N. Peranio, O. Eibl, C. Trautmann, M. Toimil-Molares, *Nucl. Instrum. Methods Phys. Res., Sect. B* **2015**, *365*, 668.
[8] G. Pennelli, *Beilstein J. Nanotechnol.* **2014**, *5*, 1268.
[9] C. J. Vineis, A. Shakouri, A. Majumdar, M. G. Kanatzidis, *Adv. Mater.* **2010**, *22*, 3970.
[10] T. M. Tritt, *Annu. Rev. Mater. Res.* **2011**, *41*, 433.
[11] G. J. Snyder, E. S. Toberer, *Nat. Mater.* **2008**, *7*, 105.
[12] B. C. Blanke, J. H. Birden, K. C. Jordan, E. L. Murphy, Nuclear battery-Thermocouple Type Summary Report, U.S. Atomic Energy Commission, Miamisburg, Ohio: Mound Laboratory **1960**, Report No.: MLM-1127.
[13] D. Beretta, A. Perego, G. Lanzani, M. Caironi, *Sustainable Energy Fuels* **2017**, *1*, 174.
[14] J. A. Lee, A. E. Aliev, J. S. Bykova, M. J. de Andrade, D. Kim, H. J. Sim, X. Leprò, A. A. Zakhidov, J.-B. Lee, G. M. Spinks, S. Roth, S. J. Kim, R. H. Baughman, *Adv. Mater.* **2016**, *28*, 5038.
[15] S. LeBlanc, *Sustainable Mater. Technol.* **2014**, *1*, 26.
[16] G. Tan, L.-D. Zhao, M. G. Kanatzidis, *Chem. Rev.* **2016**, *16*, 12123.
[17] A. Nozariasbmarz, A. Agarwal, Z. A. Coutant, M. J. Hall, J. Liu, R. Liu, A. Malhotra, P. Norouzzadeh, M. C. Oeztuerk, V. P. Ramesh, *Jpn. J. Appl. Phys.* **2017**, *56*, 05DA04.
[18] X. Lu, D. T. Morelli, Y. Xia, F. Zhou, V. Ozolins, H. Chi, X. Zhou, C. Uher, *Adv. Eng. Mater.* **2013**, *3*, 342.
[19] M. Zhou, G. J. Snyder, L. Li, L.-D. Zhao, *Inorg. Chem. Front.* **2016**, *3*, 3.
[20] D. Beretta, N. Neophytou, J. M. Hodges, M. G. Kanatzidis, D. Narducci, M. Martin-Gonzalez, M. Beekman, B. Balke, G. Cerretti, W. Tremel, A. Zevalkink, A. I. Hofmann, C. Müller, B. Dörling, M. Campoy-Quiles, M. Caironi, *Mater. Sci. Eng., R* **2018**, *138*, 100501.
[21] D. Kiefer, L. Yu, E. Fransson, A. Gómez, D. Primetzhofer, A. Amassian, M. Campoy-Quiles, C. Müller, *Adv. Sci.* **2017**, *4*, 1600203.
[22] P. Cataldi, M. Cassinelli, J. A. Heredia-Guerrero, S. Guzman-Puyol, S. Naderizadeh, A. Athanassiou, M. Caironi, *Adv. Funct. Mater.* **2019**, *30*, 1907301.

[23] O. Bubnova, Z. U. Khan, H. Wang, S. Braun, D. R. Evans, M. Fabretto, P. Hojati-Talemi, D. Dagnelund, J.-B. Arlin, Y. H. Geerts, *Nat. Mater.* **2014**, *13*, 190.
[24] R. Kroon, D. Kiefer, D. Stegerer, L. Yu, M. Sommer, C. Müller, *Adv. Mater.* **2017**, *29*, 1700930.
[25] J. Liu, M. P. Garman, J. Dong, B. v. d. Zee, L. Qiu, G. Portale, J. C. Hummelen, L. J. A. Koster, *ACS Appl. Energy Mater.* **2019**, *2*, 9.
[26] G. Zuo, X. Liu, M. Fahlman, M. Kemerink, *Adv. Electron. Mater.* **2018**, *28*, 1703280.
[27] J. Pei, X. B. Lu, B. Yu, Z. X. Yu, *Asian J. Org. Chem.* **2018**, *7*, 489.
[28] R. Kroon, D. A. Mengistie, D. Kiefer, J. Hynynen, J. D. Ryan, L. Yu, C. Müller, *Chem. Soc. Rev.* **2016**, *45*, 6147.
[29] C. Bounioux, P. Díaz-Chao, M. Campoy-Quiles, M. S. Martín-González, A. R. Goni, R. Yerushalmi-Rozen, C. Müller, *Energy Environ. Sci.* **2013**, *6*, 918.
[30] C. Cho, M. Culebras, K. L. Wallace, Y. Song, K. Holder, J.-H. Hsu, C. Yu, J. C. Grunlan, *Nano Energy* **2016**, *28*, 426.
[31] S. B. Schmidt, M. Hönig, Y. Shin, M. Cassinelli, A. Perinot, M. Caironi, X. Jiao, C. R. McNeill, D. Fazzi, T. Biskup, M. Sommer, *ACS Appl. Polym. Mater.* **2020**, *2*, 5.
[32] Y. Shin, H. Komber, D. Caiola, M. Cassinelli, H. Sun, D. Stegerer, M. Schreiter, K. Horatz, F. Lissel, X. Jiao, C. R. McNeill, S. Cimò, C. Bertarelli, S. Fabiano, M. Caironi, M. Sommer, *Macromolecules* **2020**, *53*, 13.
[33] Y. Shin, M. Massetti, H. Komber, T. Biskup, D. Nava, G. Lanzani, M. Caironi, M. Sommer, *Adv. Electron. Mater.* **2018**, *4*, 1700581.
[34] R. R. Søndergaard, M. Hösel, N. Espinosa, M. Jørgensen, F. C. Krebs, *Energy Sci. Eng.* **2013**, *1*, 81.
[35] Y. Chen, Y. Zhao, Z. Liang, *Energy Environ. Sci.* **2015**, *8*, 401.
[36] C. Bounioux, P. Díaz-Chao, M. Campoy-Quiles, M. S. Martin-Gonzalez, A. R. Goni, R. Yerushalmi-Rozen, C. Müller, *Energy Environ. Sci.* **2013**, *6*, 918.
[37] H. Yan, N. Sada, N. Toshima, *J. Therm. Anal. Calorim.* **2002**, *69*, 881.
[38] X. Zhang, X. Lu, Y. Zhen, J. Liu, H. Dong, G. Zhao, P. He, Z. Wang, L. Jiang, W. Hu, *J. Mater. Chem. C* **2014**, *2*, 5083.
[39] O. Bubnova, Z. U. Khan, A. Malti, S. Braun, M. Fahlman, M. Berggren, X. Crispin, *Nat. Mater.* **2011**, *10*, 429.
[40] B. Russ, A. Glaudell, J. J. Urban, M. L. Chabinyc, R. A. Segalman, *Nat. Rev. Mater.* **2016**, *1*, 16050.
[41] A. M. Glaudell, J. E. Cochran, S. N. Patel, M. L. Chabinyc, *Adv. Energy Mater.* **2015**, *5*, 1401072.
[42] G. Zuo, Z. Li, E. Wang, M. Kemerink, *Adv. Electron. Mater.* **2018**, *4*, 1700501.
[43] H. Mamur, R. Ahiska, *Int. J. Renewable Energy Res.* **2014**, *4*, 128.
[44] G. Kim, L. Shao, K. Zhang, K. P. Pipe, *Nat. Mater.* **2013**, *12*, 719.
[45] Z. Fan, P. Li, D. Du, J. Ouyang, *Adv. Energy Mater.* **2017**, *7*, 1602116.
[46] K. Zhang, Y. Zhang, S. Wang, *Sci. Rep.* **2013**, *3*, 3448.
[47] N. Toshima, *Macromol. Symp.* **2002**, *186*, 81.
[48] Y. Lu, J.-Y. Wang, J. Pei, *Chem. Mater.* **2019**, *31*, 6412.
[49] C.-J. Yao, H.-L. Zhang, Q. Zhang, *Polymers* **2019**, *11*, 107.
[50] M. Culebras, K. Choi, C. Cho, *Micromachines* **2018**, *9*, 638.
[51] K. Walzer, B. Maennig, M. Pfeiffer, K. Leo, *Chem. Rev.* **2007**, *107*, 1233.
[52] A. Werner, F. Li, K. Harada, M. Pfeiffer, T. Fritz, K. Leo, S. Machill, *Adv. Funct. Mater.* **2004**, *14*, 255.
[53] M. L. Tietze, B. D. Rose, M. Schwarze, A. Fischer, S. Runge, J. Blochwitz-Nimoth, B. Lüssem, K. Leo, J. L. Bredas, *Adv. Funct. Mater.* **2016**, *26*, 3730.
[54] L. M. Cowen, J. Atoyo, M. J. Carnie, D. Baran, B. Schroeder, B. C. Review, *J. Solid State Sci. Technol.* **2017**, *6*, N3080.
[55] X. Guo, A. Facchetti, T. J. Marks, *Chem. Rev.* **2014**, *114*, 8943.
[56] J. E. Anthony, A. Facchetti, M. Heeney, S. R. Marder, X. Zhan, *Adv. Mater.* **2010**, *22*, 3876.
[57] D. M. de Leeuw, M. M. J. Simenon, A. R. Brown, R. E. F. Einerhand, *Synth. Met.* **1997**, *87*, 53.
[58] T. Menke, D. Ray, J. Meiss, K. Leo, M. Riede, *Appl. Phys. Lett.* **2012**, *100*, 093304.
[59] L. Qiu, J. Liu, R. Alessandri, X. Qiu, M. Koopmans, R. W. A. Havenith, S. J. Marrink, R. C. Chiechi, J. A. Koster, J. C. Hummelen, *J. Mater. Chem.* **2017**, *5*, 21234.
[60] Z. H. Wang, K. Ichimura, M. S. Dresselhaus, G. Dresselhaus, W.-T. Lee, K. A. Wang, P. C. Eklund, *Phys. Rev. B* **1993**, *48*, 10657.
[61] F. Gao, Y. Liu, Y. Xiong, P. Wu, B. Hu, L. Xu, *Front. Optoelectron. China* **2017**, *10*, 117.
[62] D. Yuan, D. Huang, C. Zhang, Y. Zou, C. Di, X. Zhu, D. Zhu, *Appl. Mater. Interfaces* **2017**, *9*, 28795.
[63] D. Huang, H. Yao, Y. Cui, Y. Zou, F. Zhang, C. Wang, H. Shen, W. Jin, J. Zhu, Y. Diao, W. Xu, C. Di, D. Zhu, *J. Am. Chem. Soc.* **2017**, *139*, 13013.
[64] J. Liu, L. Qiu, G. Portale, M. Koopmans, G. ten Brink, J. C. Hummelen, L. J. A. Koster, *Adv. Mater.* **2017**, *29*, 1701641.
[65] J. Liu, B. van der Zee, R. Alessandri, S. Sami, J. Dong, M. I. Nugraha, A. J. Barker, S. Rousseva, L. Qiu, X. Qiu, N. Klasen, R. C. Chiechi, D. Baran, M. Caironi, T. D. Anthopoulos, G. Portale, R. W. A. Havenith, S. J. Marrink, J. C. Hummelen, L. J. A. Koster, *Nat. Commun.* **2020**, *11*, 5694.
[66] N. Cho, H.-L. Yip, J. A. Davies, P. D. Kazarinoff, D. F. Zeigler, M. M. Durban, Y. Segawa, K. M. O'Malley, C. K. Luscombe, A. K. Y. Jen, *Adv. Energy Mater.* **2011**, *1*, 1148.
[67] B. D. Naab, X. Gu, T. Kurosawa, J. W. F. To, A. Salleo, Z. Bao, *Adv. Electron. Mater.* **2016**, *2*, 1600004.
[68] Y. Zhang, H. Phan, H. Zhou, X. Zhang, J. Zhou, K. Moudgil, S. Barlow, S. R. Marder, A. Facchetti, T.-Q. Nguyen, *Adv. Electron. Mater.* **2017**, *3*, 1600546.
[69] A. Higgins, S. K. Mohapatra, S. Barlow, S. R. Marder, A. Kahn, *Appl. Phys. Lett.* **2015**, *106*, 163301.
[70] Y. Liang, Z. Chen, Y. Jing, Y. Rong, A. Facchetti, Y. Yao, *J. Am. Chem. Soc.* **2015**, *137*, 4956.
[71] H. Yan, Z. Chen, Y. Zheng, C. Newman, J. R. Quinn, F. Dotz, M. Kastler, A. Facchetti, *Nature* **2009**, *457*, 679.
[72] Z. Chen, Y. Zheng, H. Yan, A. Facchetti, *J. Am. Chem. Soc.* **2008**, *131*, 8.
[73] B. D. Naab, S. Guo, E. G. Evans, P. Wei, G. L. Millhauser, A. Kahn, S. Barlow, S. R. Marder, Z. Bao, *J. Am. Chem. Soc.* **2013**, *135*, 15018.
[74] R. Schlitz, F. G. Brunetti, A. M. Glaudell, P. L. Miller, M. A. Brady, C. J. Takacs, C. J. Hawker, M. L. Chabinyc, *Adv. Mater.* **2014**, *26*, 2825.
[75] B. D. Naab, S. Zhang, K. Vandewal, A. Salleo, S. Barlow, S. R. Marder, Z. Bao, *Adv. Mater.* **2014**, *26*, 4268.
[76] B. Saglio, M. Mura, M. Massetti, F. Scuratti, D. Beretta, X. Jiao, C. R. McNeill, M. Sommer, A. Famulari, G. Lanzani, M. Caironi, C. Bertarelli, *J. Mater. Chem. A* **2018**, *6*, 15294.
[77] S. Wang, H. Sun, U. Ail, M. Vagi, P. O. A. Persson, J. W. Andreasen, W. Thiel, M. Berggren, X. Crispin, D. Fazzi, S. Fabiano, *Adv. Mater.* **2016**, *28*, 10764.
[78] S. Fabiano, S. Braun, X. Liu, E. Weverberghs, P. Gerbaux, M. Fahlman, M. Berggren, X. Crispin, *Adv. Mater.* **2014**, *26*, 26.
[79] R. Steyrleuthner, M. Schubert, I. Howard, B. Klaumünzer, K. Schilling, Z. Chen, P. Saalfrank, F. Laquai, A. Facchetti, D. Neher, *J. Am. Chem. Soc.* **2012**, *134*, 18303.
[80] D. L. Meyer, R. Matsidik, S. Huettner, M. Sommer, T. Biskup, *Phys. Chem. Chem. Phys.* **2018**, *20*, 2716.
[81] D. Fazzi, M. Caironi, *Phys. Chem. Chem. Phys.* **2015**, *17*, 8573.
[82] D. Di Nuzzo, C. Fontanesi, R. Jones, S. Allard, I. Dumsch, U. Scherf, E. von Hauff, S. Schumacher, E. Da Como, *Nat. Commun.* **2015**, *6*, 6460.

[83] D. Fazzi, M. Caironi, C. Castiglioni, *J. Am. Chem. Soc.* **2011**, *133*, 19056.
[84] X. K. Gao, Y. B. Hu, *J. Mater. Chem. C* **2014**, *2*, 3099.
[85] K. Shi, F. Zhang, C. A. Di, T. W. Yan, Y. Zou, X. Zhou, D. Zhu, J. Y. Wang, J. Pei, *J. Am. Chem. Soc.* **2015**, *137*, 6979.
[86] D. Nava, Y. Shin, M. Massetti, X. Jiao, T. Biskup, M. S. Jagadeesh, A. Calloni, L. Duò, G. Lanzani, C. R. McNeill, M. Sommer, M. Caironi, *Appl. Energy Mater.* **2018**, *1*, 4626.
[87] J. Liu, L. Qiu, R. Alessandri, X. Qiu, G. Portale, J. Dong, W. Talsma, G. Ye, A. A. Sengrian, P. C. T. Souza, M. A. Loi, R. C. Chiechi, S. J. Marrink, J. C. Hummelen, J. A. Koster, *Adv. Mater.* **2018**, *30*, 1704630.
[88] D. Kiefer, A. Giovannitti, H. Sun, T. Biskup, A. Hofmann, M. Koopmans, C. Cendra, S. Weber, J. A. Koster, E. Olsson, J. Rivnay, S. Fabiano, I. McCulloch, C. Müller, *Energy Lett.* **2018**, *3*, 278.
[89] I. E. Jacobs, A. J. Moule, *Adv. Mater.* **2017**, *29*, 1703063.
[90] S. Wang, H. Sun, T. Erdmann, G. Wang, D. Fazzi, U. Lappan, Y. Puttisong, Z. Chen, M. Berggren, X. Crispin, A. Kiriy, B. Voit, T. J. Marks, S. Fabiano, A. Facchetti, *Adv. Mater.* **2018**, *30*, 1801898.
[91] R. Matsidik, M. Giorgio, A. Luzio, M. Caironi, H. Komber, M. Sommer, *J. Org. Chem.* **2018**, *44*, 6121.
[92] J. Liu, G. Ye, B. van der Zee, J. Dong, X. Qiu, Y. Liu, G. Portale, R. C. Chiechi, J. A. Koster, *Adv. Mater.* **2018**, *30*, 1804290.
[93] R. Kim, P. S. K. Amegadze, I. Kang, H.-J. Yun, Y.-Y. Noh, S.-K. Kwon, Y.-H. Kim, *Adv. Funct. Mater.* **2013**, *23*, 5719.
[94] I. Kang, T. K. An, J.-A. Hong, H.-J. Yun, R. Kim, D. S. Chung, C. E. Park, Y.-H. Kim, S.-K. Kwon, *Adv. Mater.* **2013**, *25*, 524.
[95] D. S. Chung, S. J. Lee, J. W. Park, D. B. Choi, D. H. Lee, J. W. Park, S. C. Shin, Y.-H. Kim, S.-K. Kwon, C. E. Park, *Chem. Mater.* **2008**, *20*, 3450.
[96] K. Park, Y. Shin, X. Jiao, C. R. McNeill, Y.-H. Kim, S.-K. Kwon, Y.-Y. Noh, *ACS Appl. Mater. Interfaces* **2019**, *11*, 35185.
[97] M. Kim, W.-T. Park, S. U. Ryu, S. Y. Son, J. Lee, T. J. Shin, Y.-Y. Noh, T. Park, *Chem. Mater.* **2019**, *31*, 4864.
[98] T. Erdmann, S. Fabiano, B. Milian-Medina, D. Hanifi, Z. Chen, M. Berggren, J. Gierschner, A. Salleo, B. Voit, A. Facchetti, *Adv. Mater.* **2016**, *28*, 9169.
[99] N. An, H. Ran, Y. Geng, Q. Zeng, J. Hu, J. Yang, Y. Sun, X. Wang, E. Zhou, *Appl. Mater. Interface* **2019**, *11*, 42412.
[100] X.-Q. Zhu, M.-T. Zhang, A. Yu, C.-H. Wang, J.-P. Cheng, *J. Am. Chem. Soc.* **2008**, *130*, 2501.
[101] P. Wei, J. H. Oh, G. Dong, Z. Bao, *J. Am. Chem. Soc.* **2010**, *132*, 8852.
[102] G. Zuo, Z. Li, E. Wang, M. Kemerink, *Adv. Funct. Mater.* **2018**, *28*, 1703280.
[103] S. S. N. Bharadwaja, C. Venkatasubramanian, N. Fieldhouse, S. Ashok, M. W. Horn, T. N. Jackson, *Appl. Phys. Lett.* **2009**, *94*, 222110.
[104] W. F. Pasveer, J. Cottaar, C. Tanase, R. Coehoorn, P. A. Bobbert, P. W. M. Blom, D. M. de Leeuw, M. A. J. Michels, *Phys. Rev. Lett.* **2005**, *94*, 206601.
[105] M. Caironi, M. Bird, D. Fazzi, Z. Chen, R. Di Pietro, C. Newman, A. Facchetti, H. Sirringhaus, *Adv. Funct. Mater.* **2011**, *21*, 3371.
[106] M. Cutler, N. F. Mott, *Phys. Rev.* **1969**, *181*, 1336.
[107] D. Beretta, A. J. Barker, I. Maqueira-Albo, A. Calloni, G. Bussetti, G. Dell'Erba, A. Luzio, L. Duò, A. Petrozza, G. Lanzani, M. Caironi, *Appl. Mater. Interfaces* **2017**, *21*, 18151.
[108] N. M. Kirby, S. T. Mudie, A. M. Hawley, D. J. Cookson, H. D. T. Mertens, N. Cowieson, V. Samardzic-Boban, *J. Appl. Cryst.* **2013**, *46*, 1670.
[109] J. Ilavsky, *J. Appl. Cryst.* **2012**, *45*, 324.
[110] D. Beretta, P. Bruno, G. Lanzani, M. Caironi, *Rev. Sci. Instrum.* **2015**, *86*, 75104.